I&EC research
Industrial & Engineering Chemistry Research

pubs.acs.org/IECR
Article

Periodic Operation of Three-Way Catalysts: From Synthetic Gas Bench Testing to Real-World Engine Performance

Daniel Hodonj, Koki Umemoto, Masato Terasawa, Zexin Yu, Uwe Wagner, Toshihiro Mori, Hiromasa Nishioka, Takao Mishima, Olaf Deutschmann, Thomas Koch, Jin Kusaka, and Patrick Lott*

Cite This: *Ind. Eng. Chem. Res.* 2025, 64, 8143−8155

ABSTRACT: This study utilized a synthetic gas test bench (SGB) and two engine test benches (ETBs) to evaluate the periodic operation of an industrially relevant three-way catalyst formulation. The goal was to bridge the gap between laboratory-scale testing and real-world applications, ensuring the reliability of catalysts in engine environments under periodic conditions. SGB testing showed significant increases in NO, CO, and hydrocarbon conversion and N_2 selectivity under dynamic operation compared to stoichiometric steady-state conditions. Despite differences in ETB testing due to the realistic conditions, notable improvements in pollutant conversion were achieved. Challenges included inaccurate control of the mean air−fuel equivalence ratio (AFR) by the engine control unit and the AFR sensor. The findings underscore the importance of harmonizing engine operation with formulation-governed catalyst properties to minimize tailpipe emissions. Periodic operation emerges as a promising technique for enhancing catalyst efficiency in varying engine conditions.

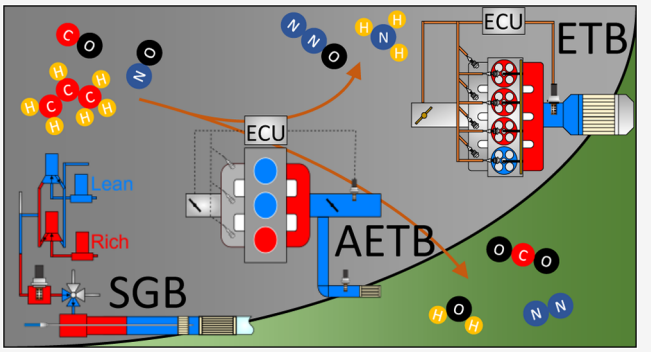

INTRODUCTION

In light of tightening global emission standards, dynamic operation of three-way catalysts (TWCs), specifically the forced alternating lean-rich cycles referred to as λ-dithering, has become a promising approach to enhance the conversion of CO, NO, and unburned hydrocarbons (HCs) from gasoline engines. Pioneering research in the 1980s by General Motors[1−5] and Toyota[6−10] focused on the periodic modulation between lean and rich exhaust gas compositions as an alternative to the conventional steady-state operation at stoichiometric air−fuel equivalence ratio (AFR) conditions. The above-mentioned studies demonstrate that an optimal frequency of lean-rich switches enhances pollutant conversion, especially that of NO, compared to the steady-state operation. The beneficial effects of periodic operation on TWC performance are most pronounced at low temperatures, below the light-off threshold of the exhaust gas pollutants,[11,12] where the reaction rate is strongly influenced by catalyst surface processes and thus chemical kinetics.[2] This aspect makes periodic operation particularly interesting for hybrid electric vehicles (HEVs), whose frequent start−stop cycles result in exhaust temperatures lower than those of conventional internal combustion engines (ICEs). However, conventional ICE vehicles can also benefit from the improved pollutant conversion of periodic operation, especially for short urban journeys when the catalyst rarely reaches its optimal operating temperature.

Although the periodic operation of TWCs has been known for some time, it is gaining popularity, as underscored by a number of recent publications.[13−19] Compared to other already fully developed emission reduction strategies, the use of advanced catalyst control strategies such as λ-dithering offers a high potential for reducing pollutant emissions without affecting the existing engine settings and run conditions; consequently, a complex feedback control system will not be required.[20] Synthetic gas test bench (SGB) experiments showed that the optimal catalyst operation and thus the maximum pollutant conversion enhancement on the catalyst are strongly influenced by operating conditions such as temperature and exhaust mass flow, parameters of the periodic operation, including frequency and amplitude, back-mixing upstream of the catalyst, and oxygen storage capacity.[17,21] However, in real-world applications, operation conditions such as exhaust gas mass flow, composition, and temperature are influenced by the operation conditions of the engine. Therefore, transferring results from the SGB to the real-world application in an engine test bench (ETB) required

Received: January 9, 2025
Revised: March 10, 2025
Accepted: March 24, 2025
Published: April 14, 2025

https://doi.org/10.1021/acs.iecr.5c00132
Ind. Eng. Chem. Res. 2025, 64, 8143−8155

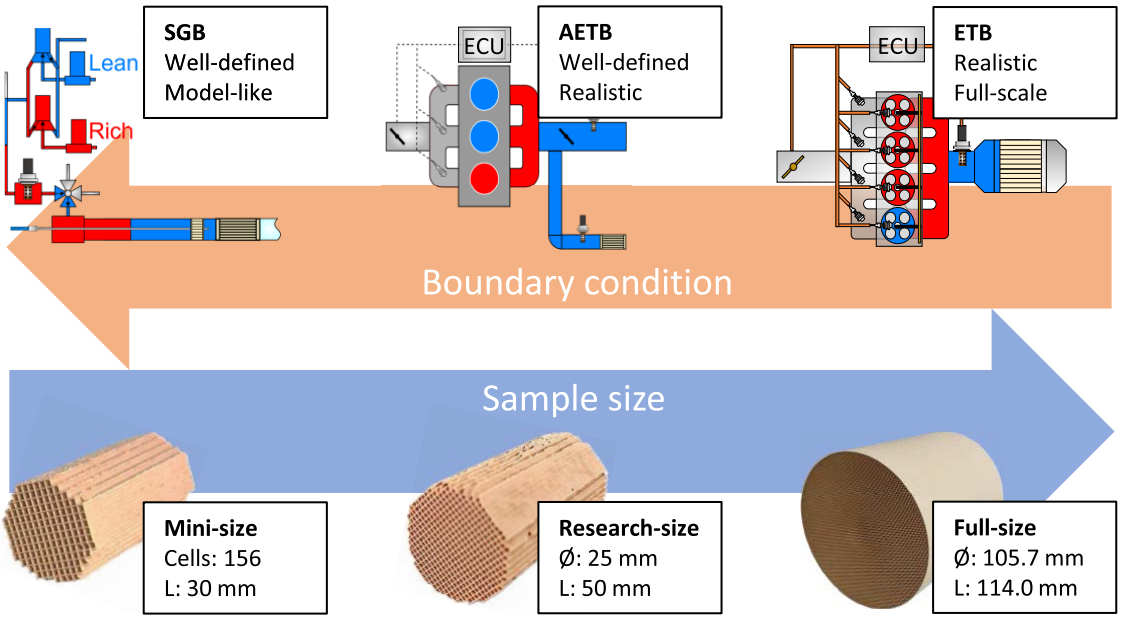

Figure 1. Overview of the research approach.

careful adjustment and validation of test conditions to account for the differences between controlled laboratory conditions and realistic engine operating conditions.

Previous SGB experiments utilized hot wire anemometry to assess amplitude deterioration due to axial dispersion at increasing frequencies.[5,22] Herz et al.[3] further demonstrated that during real engine operation, the amplitude initially decreases during lean-rich switches due to fuel spray wetting of the inlet manifold during the rich phase and subsequent evaporation during the lean phase. Additionally, Cho[1] found that the CO light-off temperature in steady-state experiments on Pt/Al_2O_3 catalysts differed by approximately 200 °C between SGB and ETB experiments, likely due to the inhibiting effects of additional components present in the real exhaust gas. Toyota researchers also investigated the influence of modulation frequency on Pt/Al_2O_3, Pd/Al_2O_3, and Rh/Al_2O_3 model catalysts in both SGB[8] and ETB[10] experiments, but meaningful comparisons between these studies remain difficult without considering differences in boundary conditions such as temperature, gas hourly space velocity (GHSV), and amplitude deterioration. Among these, Pd-based catalysts are particularly important due to their high oxidation activity for CO and unburned hydrocarbons and their sufficient NO_x reduction capability,[23] making them a cost-effective alternative to the rarer and more expensive Rh.[24] Additionally, their high hydrothermal resistance to sintering[25,26] makes Pd-based catalysts particularly suitable for close-coupled applications near the engine, where they help minimize amplitude deterioration during periodic operation.

In this context, the present study examines the periodic operation of a well-defined, industry-relevant Pd-only TWC in various sample sizes in an SGB, allowing dynamic reactor operation with a realistic exhaust gas mixture; additionally, two ETBs with different configurations are assessed. The objective is to address differences between the periodic operations of the catalyst in the SGB and ETBs, providing insights relevant to optimizing the operating strategy and confirming the efficacy of the process under real-world applications. With this, our study contributes to the efficient transfer of lab-scale knowledge into full-scale applications.

EXPERIMENTAL SECTION

Catalyst Materials and Characterization. The Pd-based monolithic catalysts (2 g_{Pd} L^{-1}) subject to the present study have already been investigated in previous studies[27,28] and were prepared using incipient wetness impregnation followed by dip coating of a cordierite honeycomb (105.7 mm diameter, 114.0 mm length, 600 cpsi, 4.3 mil from NGK Insulators). The noble metal (precursor, aqueous solution of $Pd(NO_3)_2$; Tanaka Precious Metals, Japan) is supported on a mixture of CeO_2-based mixed oxide (CZ, 98 g L^{-1}, consisting of 40 mol % Ce, 50 mol % Zr, 4 mol % La, and 6 mol % Nd; Daiichi Kigenso Kagaku Kogyo, Japan) and γ-Al_2O_3 (10 g L^{-1}, comprising 97% Al_2O_3 and 3 mol % La_2O_3; Sasol Chemical). The detailed catalyst preparation procedure is described elsewhere.[27]

To calculate the dispersion of palladium for the monolithic Pd/CZ catalyst sample, low-temperature CO chemisorption measurements based on the work of Tanabe et al.[29] were conducted in a custom-built apparatus equipped with an IR detector (X-Stream, Emerson). The sample was oxidized in a quartz glass tubular reactor (Qsil) at 500 °C with atmospheric oxygen for 20 min and subsequently reduced at 400 °C for 60 min by using 5% H_2 in N_2. Subsequently, the reactor was cooled to −77 °C in a dry ice−isopropanol bath under N_2 flushing, after which a calibration gas (100 ppm of CO in N_2) was dosed onto the catalyst. In order to evaluate the dispersion of the precious metal, the adsorption of CO was monitored. The obtained data were evaluated assuming that the adsorption ratio of CO to Pd is 1:1.[30] The average particle diameter of palladium was calculated on the assumption of a hemispherical particle geometry.[31]

Complete oxygen storage capacity (OSCC) was measured by initially oxidizing the monolithic catalyst at 550 °C with 2% O_2 in N_2 for 20 min in the SGB described below. Subsequently, the sample was cooled to different temperatures (150−550 °C) in N_2 and then reduced with 1% CO in N_2. The

https://doi.org/10.1021/acs.iecr.5c00132
Ind. Eng. Chem. Res. 2025, 64, 8143−8155

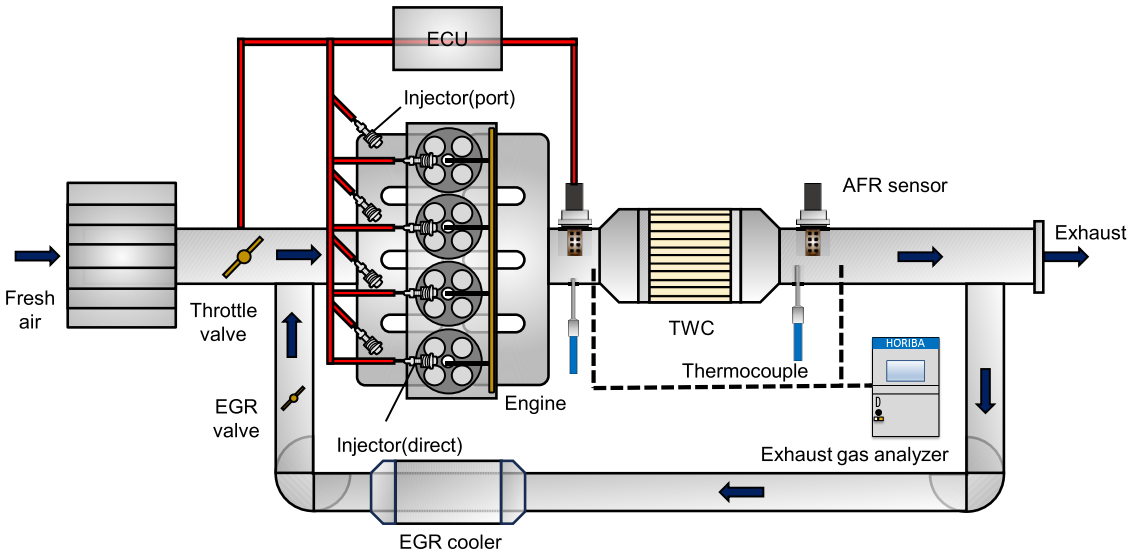

Figure 2. Schematic of the engine test bench with a full-size catalyst.

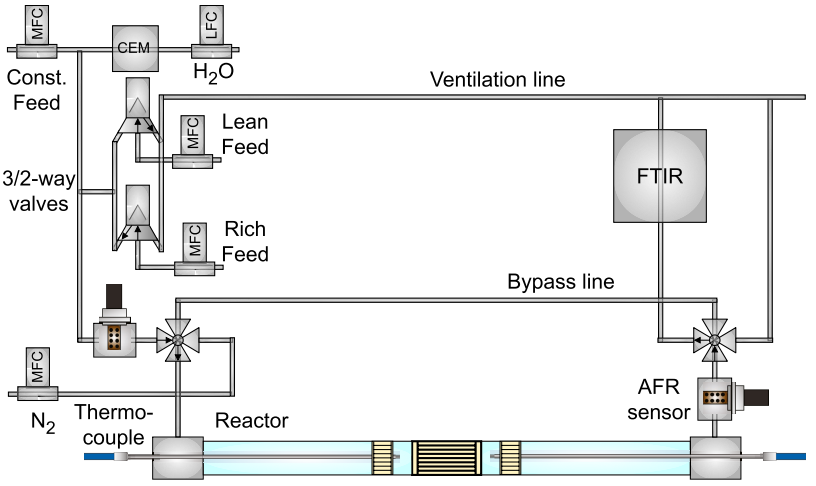

Figure 3. Schematic of the synthetic gas test bench with a mini-size catalyst.

OSCC at the respective temperature corresponds to the amount of CO_2 formed during reduction and is specified per mass of the catalyst.

Experimental Setups. Figure 1 provides an overview of the research approach chosen herein, which employs three different test benches to investigate the influence of periodic operation on the TWC. SGBs are widely used to study the catalytic activity of mini-sized catalyst samples under well-defined boundary conditions. These setups provide model-like exhaust gas compositions, allowing for a controlled evaluation of catalytic reactions without the complexities of real engine exhaust. This approach is particularly useful for investigating fundamental catalytic behaviors, addressing isolated, specific catalytic phenomena, and understanding reaction kinetics. On the other end of the spectrum, full-scale ETBs allow for the investigation of full-size TWC samples under realistic exhaust gas compositions and boundary conditions. This setup replicates actual engine operating environments, providing a direct assessment of catalyst performance in practical applications. However, due to the inherent variability of engine conditions, isolating specific catalytic effects can be more challenging compared to laboratory-scale experiments. To bridge the gap between precisely controlled laboratory experiments in well-defined conditions and real-world engine testing, an adaptive engine test bench (AETB) was employed. This hybrid system combines the strengths of both the SGB and ETB, enabling the testing of research-sized catalyst samples under realistic exhaust gas conditions while maintaining well-defined boundary conditions. By doing so, the AETB allows for a more precise evaluation of catalyst behavior under operationally relevant conditions, offering a balance between experimental control and real-world applicability.

For the experimental investigation, two identical full-size catalysts were prepared according to the methodology described in the previous section. One of these full-size catalysts was evaluated in the ETB under real engine operating conditions. From the second full-size catalyst, the research-size (50 mm length, 25 mm diameter) and mini-size samples (30 mm length, 16 mm diameter, 156 cells) were extracted from the front circumference. These extracted samples were then tested in the AETB and SGB, respectively.

Engine Test Bench. The full-size catalyst was subjected to testing on an in-line four-cylinder naturally aspirated ETB (A25A-FKS Nonhybrid, Toyota Motor Corporation) with a

https://doi.org/10.1021/acs.iecr.5c00132
Ind. Eng. Chem. Res. 2025, 64, 8143−8155

2.5 L displacement and a 13.0 compression ratio (cf. Figure 2). Both port injection and direct injection were used as fuel supply methods. Table S1 presents the fuel properties of the unleaded regular gasoline used in the ETB experiments. The full-size catalyst was wrapped with an insulation mat to prevent exhaust gas leakage, press-fitted into the canning case, and installed at the close-coupled position just below the exhaust manifold. The frequency and amplitude of dithering were controlled by adjusting the fuel injection and intake air volume with the engine control unit (ECU). Prior to testing, the catalyst was subject to an initial degreening process at an excess air ratio controlled by ECU; this process included 40 min of idle operation, followed by 1 h at 2000 rpm and 72 N m, 1 h at 2600 rpm and 139 N m, and 1 h at 3300 rpm and 175 N m.

In order to analyze the gas at the catalyst inlet and outlet, the gas analyzer (MEXA-ONE-FTIR, HORIBA) was equipped with a heated flame ionization detector (HFID), a paramagnetic detector (PMD), and a Fourier transform infrared (FTIR) spectrometer. Direct insertion-type AFR sensors (MEXA-730, HORIBA) were installed upstream and downstream of the catalyst to observe the AFR switches with a higher temporal resolution. The front AFR sensor of the ECU serves as the control device for square wave changes of the AFR value during the periodic operation. Since typically a temperature distribution in the radial direction can be expected, thermocouples were inserted at three points at the catalyst inlet (0, 24, and 48 mm from the center) and at one point at the catalyst outlet, each with a distance of 15 mm from the catalyst.

Synthetic Gas Test Bench. The mini-size monolith was evaluated in a dynamically operated in-house built synthetic gas test bench (cf. Figure 3) under precisely set reaction and exhaust gas input conditions, which is described elsewhere.[17] The mini-size monolith was wrapped in quartz glass wool and placed in a quartz glass tubular reactor (19 mm OD, 17 mm ID, 720 mm length, Qsil). The catalyst inlet temperature was measured with a thermocouple (1 mm OD, type N, TCdirect); it simultaneously served for precise control of the furnace (Gero) via a PID controller (Eurotherm). The inlet and outlet thermocouples are placed 5 mm upstream and downstream of the catalyst. The gaseous reactants and steam of the simulated exhaust gas were supplied by mass flow controllers (MFC, Bronkhorst) and a controlled evaporation mixing device (CEM, Bronkhorst), respectively, with the latter being used along with a liquid flow controller (LFC, Bronkhorst).

Figure 4 shows the O_2, CO, NO, and total hydrocarbon (THC) engine-out emissions of the above-mentioned ETB that can be equipped with the full-size catalyst during operation at steady-state conditions in the AFR range of 0.93−1.07 (symbols), along with the reactant concentration that can be set by the MFCs in the SGB (lines). The AFR value was calculated by eq 1, which was first formulated by Padeste and Baiker.[32]

$$\lambda = \frac{2O_2 + CO + 2CO_2 + H_2O + NO}{2CO + H_2 + 2CO_2 + H_2O + 9C_3H_6 + 10C_3H_8} \quad (1)$$

As underscored by the data shown in Figure 4, the AFR applied during engine operation strongly governs the raw emissions of CO and O_2. It should be noted that the slight increase of NO emission and the decrease of THC emissions with increasing AFR were not considered when simulating the exhaust gas in the SGB. Therefore, during SGB testing, the NO and THC concentration was kept constant at 1330 and 1630 ppm, respectively, which is the value obtained at $\lambda = 1$. The absolute error of this assumption within the AFR range of $\lambda = 0.932-1.068$ varied between $\Delta\lambda = -0.0029$ and 0.0026, corresponding to a relative error of −0.31 to 0.24%. This minor error is negligible, given that THC and NO concentrations fluctuate by only a few parts per million, whereas CO and O_2 concentrations are several orders of magnitude higher. The complex hydrocarbon profile of the engine exhaust was mimicked by attributing two-thirds of the THC emissions to fast oxidizing C_3H_6 and one-third to the slow oxidizing C_3H_8.[33,34] Additionally, as H_2 emissions measurements from the exhaust gas of the ETB were not accessible through FTIR and FID analyses, it was assumed for the SGB tests that the H_2 concentration was one-third of the CO concentration.[23,35] The exhaust gas simulation relied on the H_2O and CO_2 concentrations from the actual engine exhaust, which were 13 and 10%, respectively.

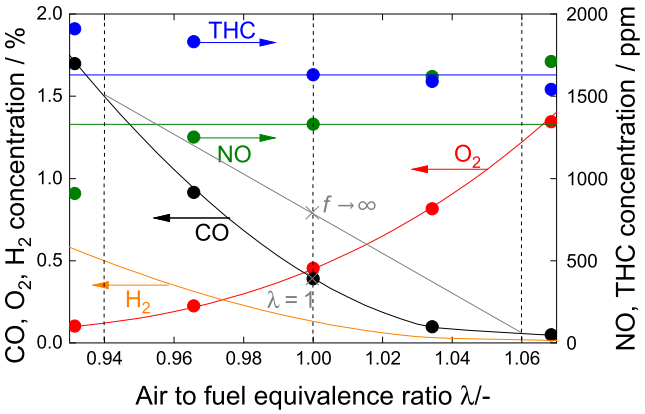

Figure 4. Comparison of CO, O_2, H_2, NO, and THC raw emissions of the ETB (symbols) and the SGB (lines) at different AFRs. $f \rightarrow \infty$ denotes the fully mixed and $\lambda = 1$ the conventional stoichiometric steady-state that is accessible by the engine. Irrespective of the AFR, the exhaust gas mixture contains 13% H_2O and 10% CO_2 and is balanced by N_2 to keep the gas hourly space velocity of 100,000 h^{-1} during SGB testing.

The forced periodic dosing of the components CO, H_2, and O_2 was achieved by using two fast-switching three-way two-position valves (Type 6624, Bürkert). These valves alternately introduce lean and rich mixtures with a frequency of up to 2.5 Hz into the reactor and the ventilation system, respectively. The test environment and capabilities of the SGB were evaluated in a previous study,[17] which excluded the occurrence of gas-phase reactions in stoichiometric exhaust gas mixtures by conducting light-off experiments up to 600 °C. Additionally, the response of the AFR sensors and the FTIR analyzer to a step change in CO concentration was studied with an uncoated honeycomb. The results showed that an almost ideal step change could be achieved and that the applied frequency did not influence the average CO concentration supplied to the reactor.

As proposed by Rappé et al.,[36] prior to the evaluation of the catalytic activity, the monolithic catalyst was degreened at 600 °C for 4 h in 10% CO_2 and 10% H_2O. The cycle-averaged conversion of the species CO, NO, C_3H_6, C_3H_8 and the selectivity to the products NH_3, N_2O, and NO_2 were calculated by integration of the concentration profiles measured by FTIR spectroscopy (MultiGas 2030, MKS Instruments), and the

https://doi.org/10.1021/acs.iecr.5c00132
Ind. Eng. Chem. Res. 2025, 64, 8143−8155

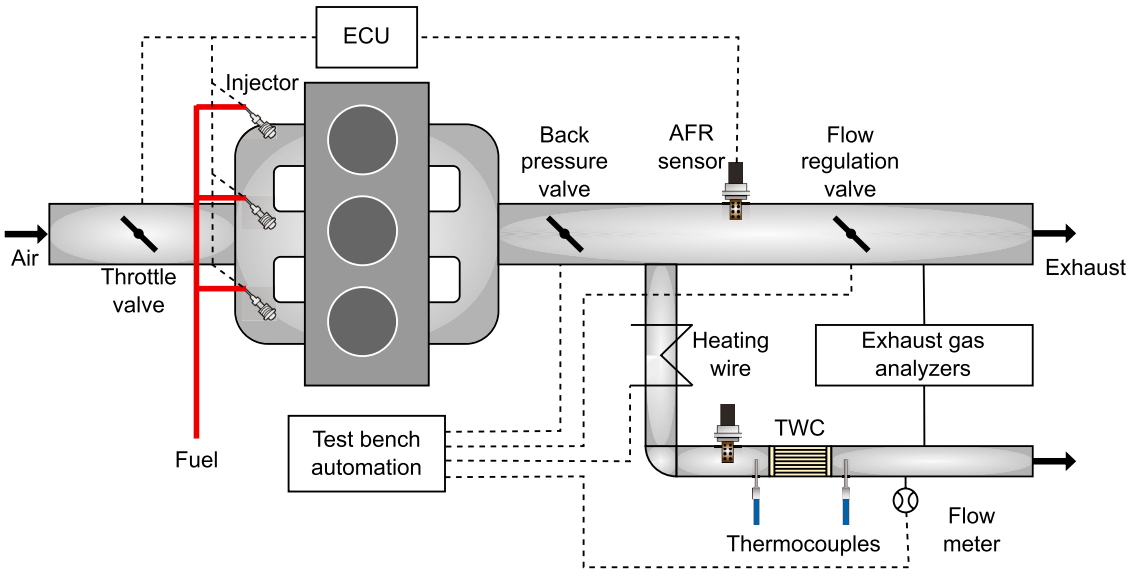

Figure 5. Schematic of the adaptive engine test bench with a research-size catalyst.

selectivity of the IR-inactive species N_2 was calculated from a balance of all nitrogen-containing species. Changes in the AFR applied to the catalyst were monitored by using AFR sensors (LSU4.9, Bosch) at the inlet and outlet of the reactor.

In order to assess whether the periodic operation is beneficial, the catalyst was analyzed under conventional stoichiometric steady-state conditions ($\lambda = 1$) and fully mixed stoichiometric steady-state conditions ($f \rightarrow \infty$). The latter was achieved by feeding the cycle-average inlet concentration of the lean and rich exhaust into the reactor, which simulates the catalyst conditions at high frequencies and complete deterioration of the applied amplitude due to mixing in the exhaust line.

Adaptive Engine Test Bench. Figure 5 depicts the schematic of the adaptive engine test bench consisting of the engine and the sample catalyst partial flow system. The test engine is based on a 2.2 L, in-line three-cylinder CNG engine with a compression ratio of 11.0.[37,38] Each inlet port of the engine is additionally fitted with gasoline injectors (EV14, Bosch) to enable periodic gasoline operation. Table S2 presents the fuel properties of the unleaded premium gasoline used in the AETB experiments. After the exhaust manifold, a smaller diameter bypass pipeline was connected to the exhaust pipe to enable testing of the research-sized catalyst samples.

The adaptive control of the exhaust gas flow, temperature, and pressure in the bypass line and thus at the research-size catalyst sample was achieved by means of a flow regulation valve, electrical heating wires, and a back-pressure valve, which was controlled by test bench automation. An AFR sensor (LSU4.2, Bosch) was installed in the main exhaust pipe to control the periodic operation with the ECU, which provides a function for automatic AFR variation. A second AFR sensor was placed directly upstream of the catalyst sample to monitor the forced AFR fluctuation in front of the sample. Moreover, thermocouples were utilized to monitor the temperature of the exhaust gas upstream and downstream of the catalyst probe, maintaining a distance of 20 mm between the probes and the sample. The concentration of the exhaust gas upstream and downstream of the catalyst sample was determined using an FTIR spectrometer (MultiGas 2030, MKS Instruments) and an exhaust gas analyzer (AMA 4000, AVL).

Figure 6 illustrates the exhaust gas composition of the engine equipped with the sample holder within the AFR range of

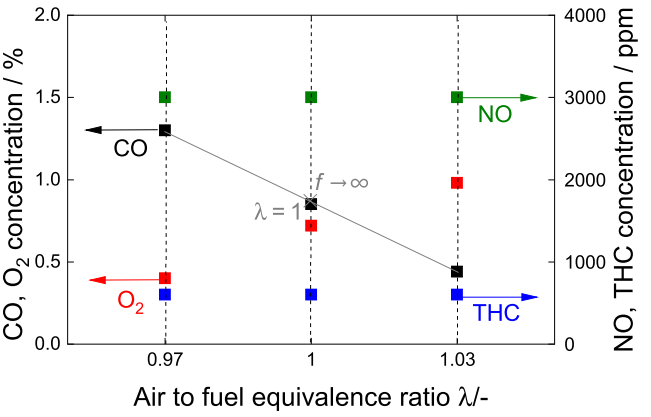

Figure 6. CO, O_2, NO, and THC raw emissions of the AETB (points) at different AFRs. Due to the low amplitude, the pollutant concentration was similar for fully mixed ($f \rightarrow \infty$) and conventional stoichiometric steady-state ($\lambda = 1$) operations. Irrespective of the AFR, the exhaust gas mixture contained 13% H_2O and 14% CO_2.

0.97−1.03. Notably, the NO emissions are elevated, while the THC emissions are diminished in comparison to the other ETB, which may be attributed to disparate operational cycles of the engines. Furthermore, the concentrations of gaseous species for the fully mixed steady-state ($f \rightarrow \infty$) and the conventional steady-state ($\lambda = 1$) coincide due to the narrow AFR range in the engine, which can also be observed in the exhaust gas composition of the other engine at small amplitude.

RESULTS AND DISCUSSION

Catalyst Characterization. It has been reported that conventional CO chemisorption measurements of noble metals supported on an oxygen storage material (OSM) result in an overestimation of the dispersion and thus an underestimation of the precious metal particle diameter due to spillover effects between the noble metal and the OSM.[29,39]

https://doi.org/10.1021/acs.iecr.5c00132
Ind. Eng. Chem. Res. 2025, 64, 8143−8155

Consequently, a low-temperature CO chemisorption method was employed in this study, which revealed an average particle size of 11 nm. This is in good agreement with the results measured by the CO_2 preinjection technique at 50 °C (12 nm) for the same catalyst sample[27] and for samples with comparable Pd loadings.[40]

Table 1 shows the increasing OSCC with increasing reduction temperature, which is in line with previous observations as well.[41] Using the same catalyst formulation as subject to our present study, Machida et al.[27] obtained a dynamic OSC of 410 μmol g^{-1} when evaluating AFR sensor data of slow lean to rich switches at 450 °C on an engine dynamometer. The lower values of the dynamic OSC measurement at temperatures higher than 300 °C are in agreement with the literature findings and can be attributed to the fact that the OSCC is related to the total reducibility measured at thermodynamic equilibrium, whereas the dynamic OSC rather corresponds to the rate of oxygen release from the material, which is a kinetic phenomenon.[42] Moreover, the reductive chemical potential in the presence of H_2O and CO_2 in a real exhaust gas is lower, which consequently reduces the available amount of oxygen.[43,44] These material properties are of high relevance during the interpretation of the following activity data.

Table 1. OSCC of Pd/CZ at Different Reduction Temperatures

T_{red} (°C)	150	250	350	450	550
OSCC (μmol g^{-1})	227	524	616	711	772

SGB Results. An SGB provides a controlled catalyst testing environment with precisely set inlet temperatures, gas mixtures, and GHSVs, allowing the evaluation of catalyst activity under steady-state and transient conditions. Figure 7 compares the pollutant conversion and the selectivity of species derivatives from NO_x at different frequencies and inlet temperatures at a constant GHSV of 100,000 h^{-1} and an amplitude A of 0.06 under the fully mixed stoichiometric steady-state ($f \to \infty$) and conventional stoichiometric steady-state ($\lambda = 1$) conditions.

The conversion of CO and C_3H_6 obtained under fully mixed and conventional stoichiometric steady-state conditions exhibits similar behavior. However, full conversion of NO_x and C_3H_8 can be achieved at 300 °C under fully mixed steady-state conditions, whereas 400 °C is required under conventional steady-state conditions. These trends are in agreement with measurements of Padeste and Baiker[32] on $Pt-Rh/Al_2O_3$ and $Pt-Rh/CeO_2-Al_2O_3$ TWC samples. The higher partial pressure of O_2, CO, and H_2 at the catalyst inlet under the fully mixed stoichiometric steady-state condition compared to the conventional stoichiometric steady-state condition (cf. Figure 4) increases the reaction rates of C_3H_8 and NO_x conversion, as they act as oxidizing and reducing agents, respectively. Furthermore, higher partial pressures of the reactants result in a higher adiabatic combustion temperature for $f \to \infty$, which increases the average catalyst temperature (cf. Figure 8b) and consequently increases pollutant conversion.

The secondary emissions of NH_3 and N_2O are affected by the different light-off temperatures of NO_x. In agreement with the higher NO_x light-off temperature, N_2O emissions can be observed over a larger temperature window for the conventional stoichiometric steady state (cf. Figure 7, T = 150−350 °C) compared to the fully mixed stoichiometric steady state (cf. Figure 7, T = 150−250 °C). Furthermore, for $f \to \infty$, NH_3 emissions can be observed over a wide temperature range. While at low temperatures, the direct reduction of NO by hydrogen accounts for NH_3 formation,[45,46] H_2 from the feed gas becomes increasingly consumed with increasing temperatures. The NH_3 concentrations at high temperatures are a

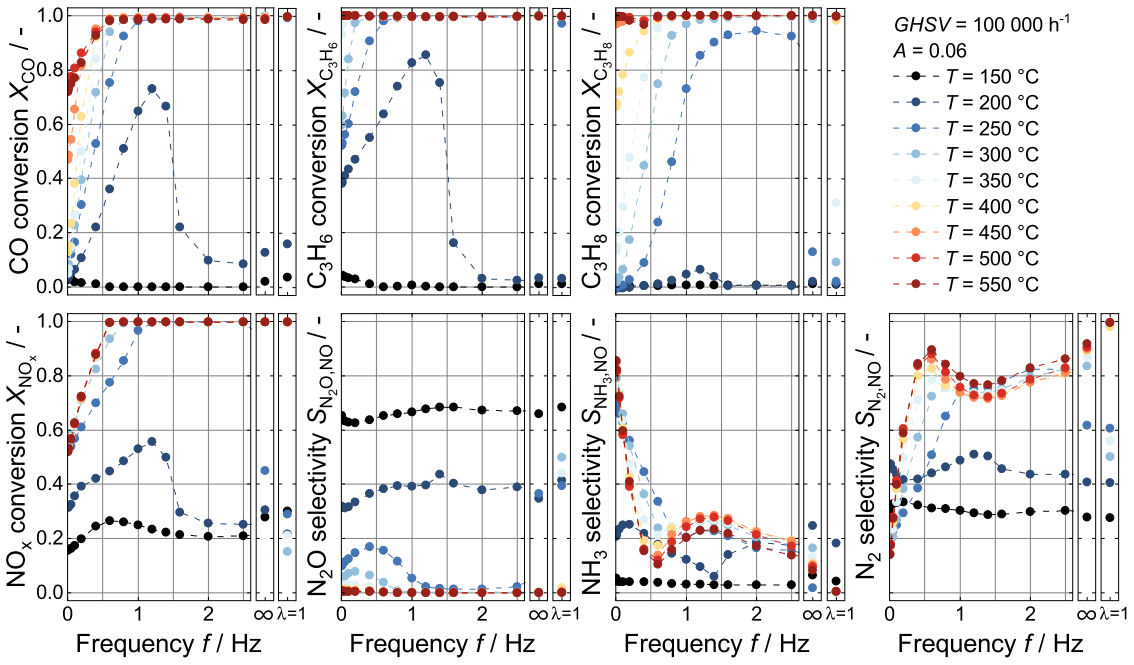

Figure 7. Cycle-average conversion of CO, C_3H_6, C_3H_8, and NO_x and selectivity to N_2O, NH_3, and N_2 derived from NO_x reduction at different inlet temperatures and frequencies in the SGB at GHSV = 100,000 h^{-1} and A = 0.06 compared to fully mixed ($f \to \infty$) and conventional ($\lambda = 1$) stoichiometric steady-state operations. Exhaust gas mixtures are depicted in Figure 4.

https://doi.org/10.1021/acs.iecr.5c00132
Ind. Eng. Chem. Res. 2025, 64, 8143−8155

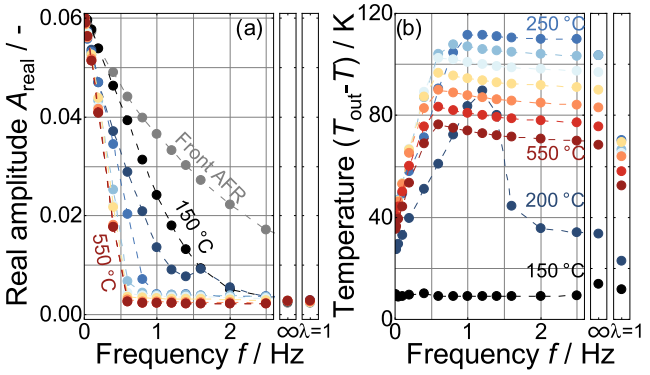

Figure 8. (a) Real amplitude at the front (temperature independent) and rear AFR sensor at different temperatures and frequencies. (b) Cycle-average temperature difference between outlet and inlet thermocouples at different frequencies and temperatures at GHSV = 100,000 h^{-1} and A = 0.06.

result of the reaction between NO and H_2 originating from the steam reforming of hydrocarbons.[23] In contrast, during λ = 1 operation, NH_3 emissions were observed only at low temperatures (cf. Figure 7). The absence of NH_3 emissions at high temperatures during conventional stoichiometric steady-state operation may be due to small deviations in the set gas concentrations. Although a stoichiometric reaction mixture can be precisely controlled through the flow rate of individual species using mass flow controllers, Wang et al.[34] and Getsoian et al.[47] demonstrated that, besides pollutant conversion, the secondary emissions of N_2O and NH_3 are highly sensitive to slight variations in the AFR around λ = 1. Additionally, the partial pressure of each species strongly influences the formation of secondary emissions, as demonstrated by calculations performed by Qian et al.[48]

The periodic operation of the monolithic catalyst sample at a temperature of 200 °C and an optimal frequency of 1.2 Hz increases the CO and C_3H_6 conversion by 50 and 90%, respectively, compared to conventional stoichiometric steady-state operation. Moreover, C_3H_8 and NO_x conversions are increased by 90 and 70% at a temperature of 250 °C and an optimal frequency of 2 Hz. This pronounced activity boost can be explained by surface phenomena. While the catalyst surface is poisoned by CO adsorbates[49] and O adsorbates[50] under steady-state conditions, periodic operation enables a change between an oxygen-dominated surface under lean conditions and a CO-dominated surface under rich conditions; the periodic lean-rich switches regularly create free surface sites, thereby increasing the reaction rate for the pollutant gas conversion.[17,49] In our previous study, we investigated a Pd/Al_2O_3-based monolithic catalyst under the same conditions as in the present study and observed the optimal frequency at 1.6 Hz.[17] The difference can be attributed to the higher oxygen storage capacity of the industrially relevant catalyst used in this study, as previously reported.[6,32] This is due to the prolonged time required for the attainment of the optimal surface composition on the noble metal, as the storage effects on the CeO_2 support decelerate the desorption process subsequent to the concentration switch.

Furthermore, periodic operation seems to reduce the N_2O selectivity for temperatures between 250 and 400 °C compared to the conventional stoichiometric steady-state. While the formation of NH_3 emission is suppressed at 250 °C, periodic operation promotes the NH_3 selectivity at higher temperatures. Consequently, N_2 selectivity reaches only 100% at the stoichiometric steady-state condition at a temperature of 550 °C. Large amounts of NH_3 are generated at low frequencies due to prolonged periods under rich conditions. At the same time, NO_2 formation (cf. Figure S1) occurs due to extended durations under lean conditions, but overall low concentrations of a maximum of 45 ppm of NO_2 were observed at low frequencies. It is possible to enhance N_2 selectivity by up to 35% by implementing periodic operation within the temperature range of 250−350 °C. As previously reported, the optimal frequency for maximal pollutant conversion depends on the time for the transition between lean and rich conditions,[51,52] which is influenced by various operating parameters such as temperature, GHSV, amplitude, the oxygen storage capacity of the catalyst, and back-mixing in the exhaust gas line.[17]

The multitude of the mutually overlapping above-mentioned effects necessitates matching the exhaust tract with the catalyst formulation when designing a periodically operated exhaust gas after-treatment system. This becomes particularly evident in Figure 8a, which depicts the amplitude monitored by front and rear AFR sensors at the reactor inlet and outlet, respectively. Note that the front AFR sensor is located upstream of the furnace and is therefore not affected by different reactor operating temperatures or reaction heat. Although the 3/2-way valves that enable the lean-rich switches are mounted only approximately 30 cm upstream of the front AFR sensor and both are connected with a comparably small stainless steel pipe (6 mm OD, 4 mm ID), a significant reduction in the set amplitude can be observed. This reduction can be attributed to two factors: the stronger back-mixing of the lean and rich phase upstream of the catalyst with increasing frequency due to axial dispersion[8] and the nonideal concentration step-changes caused by the closing and opening time of the valves of approximately 10 ms. Given a distance of about 80 cm between the AFR sensor and the catalyst sample, the actual amplitude in front of the catalyst is expected to be even smaller. The amplitude of the rear AFR sensor is additionally affected by the additional passage and mixing of the gas flow through the reactor and the catalyst honeycomb. As the pollutant conversions are low at a temperature of 150 °C (cf. Figure 7), the rear AFR sensor shows the deterioration of the amplitude after the reactor with only minor bias by the reaction. Consequently, the actual amplitude reaching the catalyst and governing its activity must therefore be between the values of the front AFR and the rear AFR sensor at 150 °C (cf. Figure 8a, black and gray lines). As the temperature increases, the conversion of pollutants increases, causing the AFR to reach unity during periodic operation, as the excess reducing agents and oxidizing agents are converted during the subsequent rich and lean phases.

The effect of the periodic operation on the catalyst temperature can be seen in Figure 8b, which shows the cycle-average temperature difference between the catalyst outlet and the inlet at different inlet temperatures and frequencies. The temperature difference of 10 K at the lowest inlet temperature of 150 °C can be attributed to a nonisothermal temperature profile in the catalyst sample. At a temperature of 200 °C, the highest temperature difference between the inlet and outlet of 89 K is achieved at 1.2 Hz, which is the optimal frequency for maximal conversion of CO and C_3H_6 (cf. Figure 7). The system undergoes self-amplification as the reaction rate further increases due to the

https://doi.org/10.1021/acs.iecr.5c00132
Ind. Eng. Chem. Res. 2025, 64, 8143−8155

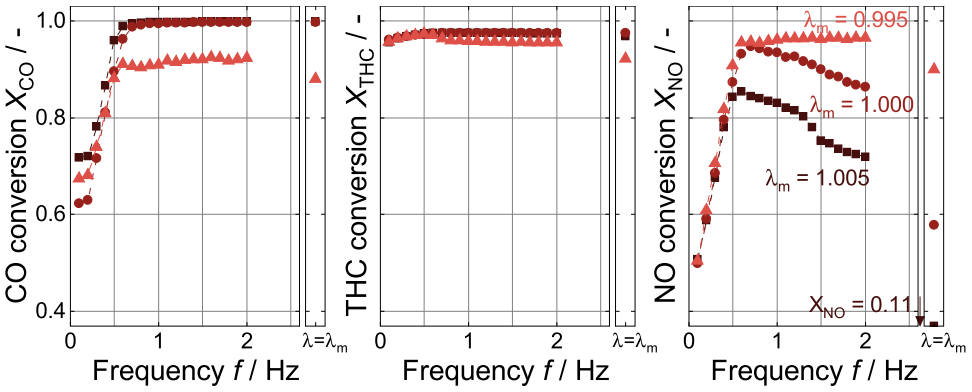

Figure 9. Cycle-average conversion of CO, THC, and NO at different frequencies and mean AFR values over the full-size monolith in the ETB at T = 580 °C, GHSV = 130,000 h^{-1}, and A = 0.06 compared to conventional steady-state conditions $\lambda = \lambda_m$. Exhaust gas mixtures are depicted in Figure 4.

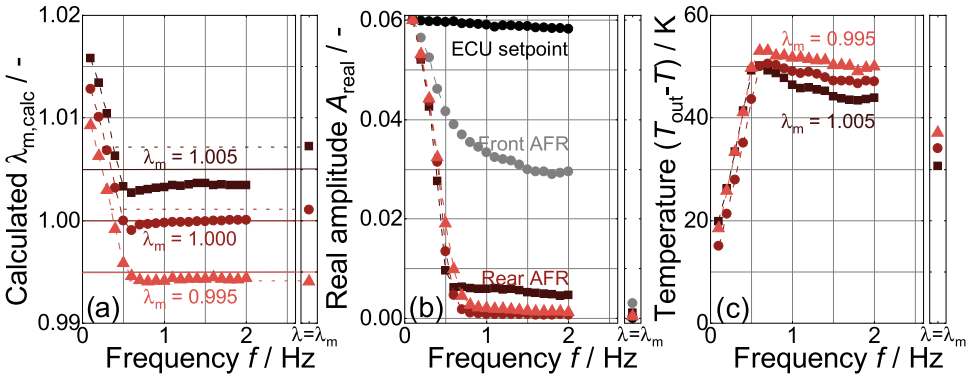

Figure 10. (a) Comparison of set mean AFR values (lines) and calculated mean AFR values (points) of the cycle-average catalyst outlet concentration using eq S1. (b) Set-point of ECU and real amplitude at the front and rear AFR sensors. (c) Cycle-average temperature difference between the average inlet temperature of the inlet thermocouples and the outlet temperature at different frequencies and mean AFR values at GHSV = 130,000 h^{-1}, T = 580 °C, and A = 0.06.

elevated average temperature within the monolith. Thus, periodic operation allows for rapid heating of the catalyst during a cold start, ensuring that operating temperatures sufficient for effective pollutant conversion are reached more quickly. At a temperature of 250 °C, a temperature difference plateau of 110 K evolves with increasing frequencies because almost full conversion of all pollutant gases is achieved. As the inlet temperature further increases, the maximum temperature difference decreases due to greater heat loss from the furnace to the environment at higher temperature levels but the aforementioned plateau remains.

ETB Results. To gain a comprehensive understanding and validation of the periodic operation under real-world conditions, testing has been conducted with the full-size catalyst mounted in a close-coupled position in the ETB. Figure 9 compares the pollutant conversion at different frequencies and mean AFR values λ_m at an amplitude of 0.06 set on the ECU with the conventional steady-state operation at high load conditions of 77.5%, resulting in a GHSV of 130,000 h^{-1} and an exhaust gas inlet temperature of 580 °C averaged across the diameter. In accordance with the findings of previous research,[47] the conversion of pollutant gases is significantly influenced by the mean AFR value at conventional steady-state conditions. For instance, under slightly lean steady-state conditions (cf., Figure 9, λ_m = 1.005), only 11% of NO can be converted. Conversely, under slightly rich conditions (λ_m = 0.995), CO and THC slip occurs and the CO and THC conversion decreases below 90 and 95%, respectively.

In contrast to the conventional stoichiometric steady-state results of the SGB (Figure 7, λ = 1, T = 550 °C), it is not possible to achieve NO full conversion in the ETB (Figure 9, $\lambda_m = \lambda$, T = 580 °C) under comparable conditions, as it was not possible to precisely set a mean AFR value of λ_m = 1.000 under conventional stoichiometric steady-state conditions with the ECU. This is underlined by the data shown in Figure 10a, which compares the calculated mean AFR values of the cycle-average catalyst outlet concentration using eq 1 with the set mean AFR values (straight lines). Consequently, the higher actual mean AFR value resulted in a particularly low NO conversion of 60% (cf. Figure 9) due to the excess of oxygen. Operating the engine around true stoichiometry is challenging, especially due to sensor deception resulting from the different diffusion rates of H_2 and hydrocarbons, which can mislead the sensor into measuring an AFR value different from the true chemical AFR.[53,54]

During periodic operation, the ETB with the full-size TWC shows the same general trends as the SGB results at T = 550 °C. The data substantiate that the THC conversion is largely independent of the applied frequency, whereas the conversion of CO and NO is significantly affected by frequency. As a consequence of the prolonged exposure to lean and rich conditions at low frequencies, CO slip occurs under rich conditions and NO slip occurs under lean conditions due to

https://doi.org/10.1021/acs.iecr.5c00132
Ind. Eng. Chem. Res. 2025, 64, 8143−8155

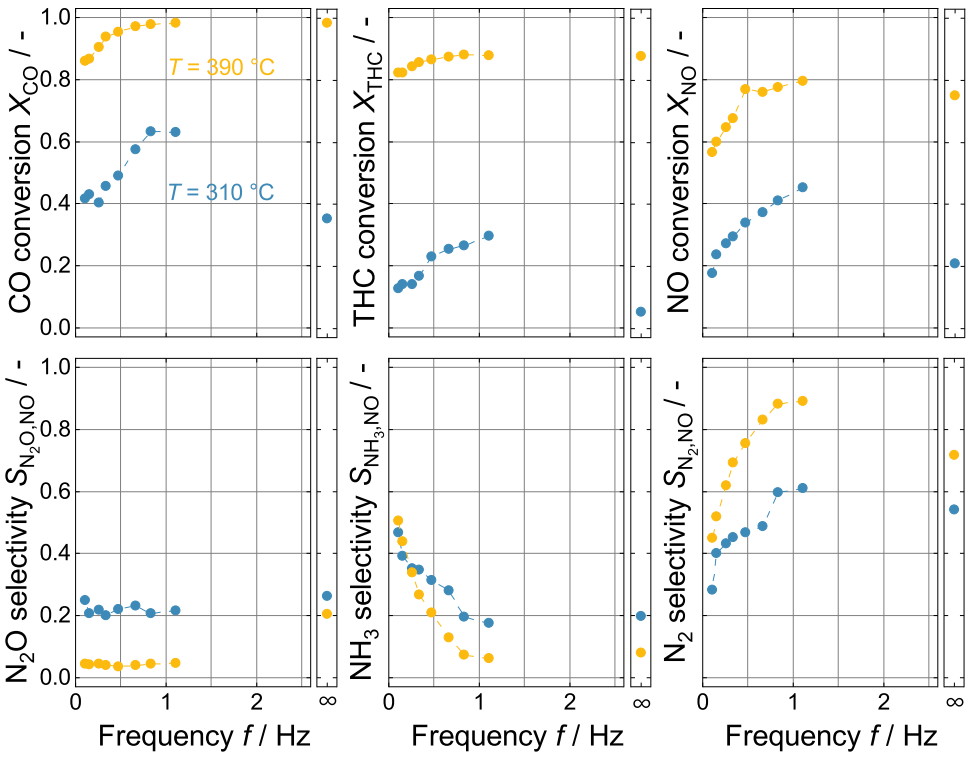

Figure 11. Cycle-average conversion of CO, THC, and NO and selectivity to N_2O, NH_3, and N_2 derived from NO reduction at different inlet temperatures and frequencies over a research-size monolith in the AETB at GHSV = 125,000 h^{-1} and A = 0.03 compared to the stoichiometric steady-state operation ($f \rightarrow \infty$). Exhaust gas mixtures are depicted in Figure 6.

the deficiency of oxidizing and reducing agents, respectively.[4,9,55,56] Conversely, at elevated temperatures, hydrocarbons can be oxidized under lean conditions and converted via steam reforming under rich conditions.[23,47] As the frequency increases, the conversion of CO and NO initially improves, with NO conversion under periodic conditions notably surpassing the performance observed under a conventional stoichiometric steady-state operation. A further increase of the frequency leads to a decrease in the NO conversion for a mean AFR value of λ_m = 1.000 and λ_m = 1.005 for frequencies above 0.6 Hz. However, SGB data and literature[11,12] suggest that at elevated temperatures, full conversion of the reactant is already achieved under stoichiometric steady-state conditions. As a result, periodic operation of the system does not lead to any further improvement in catalyst performance, and no optimal frequency exists.

The observed optimal frequency of NO conversion during the ETB experiments can be explained by the variation in the mean AFR value with frequency (cf. Figure 10a). Note that NH_3 measurements were not possible in the ETB and thus a NH_3 selectivity of 0% was considered for the mean AFR calculation of the ETB data. However, in order to account for the potential influence of NH_3 formation at low frequencies, which was observed in the SGB experiments, the maximum error was estimated. In particular, 100% NH_3 selectivity was assumed and the resulting mean AFR of the ETB data was calculated according to eq S1; a significant impact of the mean AFR values that would change the interpretation can be excluded (cf. Figure S2).

Maintaining a constant mean AFR value was not possible, thereby influencing the results at each frequency. For instance, the highest NO conversions observed at mean AFR values of λ_m = 1.005 and λ_m = 1.000 and a frequency of 0.6 Hz (cf. Figure 9) agree with the minima in the calculated mean AFR values (cf. Figure 10a). Therefore, it is evident that parts of the enhancement in the NO conversion during periodic operation can be attributed to deviations in the mean AFR value when the frequency varies. Conversely, a portion of the observed increase in NO conversion cannot be attributed to the different mean AFR values set in the ECU but is instead caused by the enhancing effect of periodic operation, which is apparent when comparing the NO conversion (cf. Figure 9) at steady-state conditions with periodic operation at the same calculated mean AFR value (cf. dotted lines, Figure 10a). When mean AFR values of 1.005, 1.000, and 0.995 are set, an increase in NO conversion of 57−67% at 0.3−0.4 Hz, 22−29% at 0.4−0.5 Hz, and 5−7% at 0.7−2 Hz can be observed, respectively, compared to the conventional steady-state. Therefore, periodic operation can significantly increase the AFR window,[11] which reduces the reliance on the AFR sensor and feedback control and minimizes the pollutant slip when the control erroneously deviates from the stoichiometric point.

Figure 10b depicts the amplitude measured at the front and rear AFR and the set-point of the ECU. At high frequencies, the set-point of the amplitude decreases slightly, which can be attributed to the limited temporal resolution of the inlet AFR function. The amplitude at the front AFR, which is mounted directly in front of the catalyst and used for ECU control, decreases due to axial dispersion in the exhaust manifold. The ETB equipped with the full-size catalyst mounted in a close-coupled position results in less back-mixing of the rich and lean exhaust gas at high frequencies compared to the SGB. For example, at 2 Hz, an amplitude of 0.03 can still be achieved, whereas, only an amplitude of 0.022 arrives at the front AFR sensor with the SGB, with the actual amplitude arriving at the catalyst being between 0.005 and 0.022 (cf. Figure 8a, black

https://doi.org/10.1021/acs.iecr.5c00132
Ind. Eng. Chem. Res. 2025, 64, 8143−8155

and gray lines). The close coupling of the catalytic converter thus ensures low-mixing operation even at very high frequencies, making a wide frequency range accessible for the exhaust gas after-treatment system, which is important due to the dependence on the operating conditions and formulation of the catalyst.[17] Analogous to the results obtained during SGB testing, high pollutant gas conversions are accompanied by high outlet temperatures originating from the exothermic nature of the chemical reaction (Figure 10c). This exothermicity allows the full-scale catalyst to heat up more quickly during periodic operation compared to conventional steady-state operation (cf. Figure 10c), which makes periodic operation an interesting approach, especially for reducing emissions during cold start.

AETB Results. In order to investigate periodic operation at lower temperatures while still facilitating the utilization of real exhaust gas and precise control of GHSV, as well as temperature and pressure at the catalyst, a research-sized catalyst was tested in an AETB under low load conditions (18.5%). Figure 11 displays the pollutant conversion and product selectivity of NO derivatives at inlet temperatures of 310 and 390 °C and different frequencies at a GHSV of 125,000 h^{-1} and an amplitude A of 0.03. It is important to note that the exhaust gas composition of the AETB (shown in Figure 6) differs from the ETB and SGB exhaust gas composition (cf. Figure 4) due to the different combustion cycles. Moreover, as a result of the convex nature of the AFR-dependent exhaust gas concentration (cf. Figure 4), the exhaust gas concentration at fully mixed steady-state conditions approaches the concentration at conventional steady-state conditions with a decrease in amplitude.

Despite the different exhaust gas compositions, the light-off temperatures of THC and NO in the AETB experiments correspond to the light-off temperatures of C_3H_8 and NO found during SGB testing of the mini-size catalyst under conventional stoichiometric steady-state conditions. In contrast, CO is already fully converted at 250 °C during the SGB tests (cf. Figure 7), whereas in the real exhaust gas mixture full CO conversion is not yet achieved at 390 °C. The literature discusses differences in light-off temperatures of up to 150 °C between real and simulated exhaust gases.[1] The differences observed herein may be attributed to varying pollutant gas concentrations, different water concentrations, and the presence of catalyst poisons, such as sulfur, in the fuel.[1,57] In addition, using solely the hydrocarbons propane and propylene in the synthetic exhaust gas cannot accurately replicate the complex light-off behavior of the hydrocarbon mix present in the real exhaust of gasoline engines that typically comprises long- and short-chain alkanes, alkenes, carbonyls, and aromatics.[58] As the temperature increases from 310 to 390 °C, the selectivity to N_2O decreases from 26 to 20% and that to NH_3 decreases from 20% to 8% at the AETB at stoichiometric steady-state conditions. Although the actual values differ, the decline in N_2O and NH_3 selectivity is consistent with the findings of the SGB under conventional and fully mixed stoichiometric steady-state conditions within the same temperature range. The varying selectivity can be attributed to different NO conversions in AETB and SGB and the sensitivity of secondary emission formation on the AFR value around stoichiometry,[34,47] which enables water gas shift reactions to take place at slightly rich conditions.[23]

At 310 °C and a frequency of 1.1 Hz, an increase of more than 24% in the pollutant conversion of CO, NO, and THC and 8% in the N_2 selectivity can be observed compared to the stoichiometric steady-state conditions (cf. Figure 11), which is consistent with the observed temperature and frequency range for conversion enhancement induced by periodic operation in the SGB. At 390 °C, the enhancement resulting from periodic operation at 1.1 Hz in comparison to stoichiometric steady-state conditions is reduced to 5% for the NO conversion, whereas N_2 selectivity is increased by 15%. It should be noted that the AETB can only be operated up to a frequency of 1.1 Hz, as the amplitude at the ECU set-point deviates by more than 10% from A = 0.03 above this frequency, as can be seen in Figure 12a (black line). The observed increase in pollutant

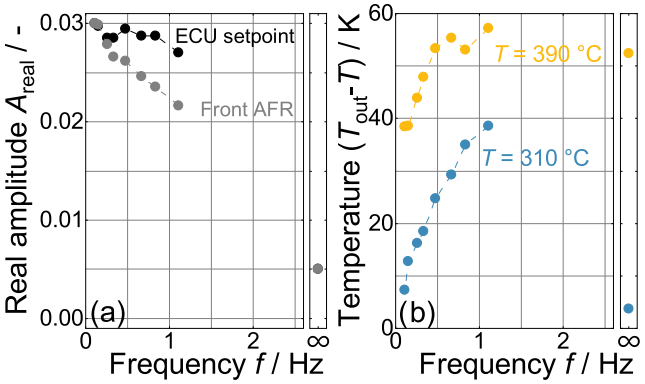

Figure 12. (a) Control amplitude of ECU and real amplitude at the front AFR at different frequencies. (b) Cycle-average temperature difference between outlet and inlet thermocouples at inlet temperatures of 310 and 390 °C and different frequencies.

conversion up to 1.1 Hz, along with the significant decrease in NH_3 selectivity and the nearly frequency-independent N_2O selectivity (cf. Figure 11), aligns with the findings from the SGB experiments. Although the improvement to the fully mixed stoichiometric steady-state indicates the existence of an optimal frequency, no optimal frequency can be determined due to the limited frequency range of the AETB. The optimal frequency of 2 Hz observed in the SGB results at 250 °C indicates that the optimal frequency on the AETB must be at an even higher frequency due to the higher temperatures and GHSV in the AETB experiments. Furthermore, the diminished volume between the engine and the catalyst results in a reduction in back-mixing within the exhaust gas line of the AETB compared to the SGB and ETB. For instance, the amplitude deterioration at the catalyst inlet for the AETB is 27% at 1.1 Hz (cf. Figure 12a, gray line); this is less severe than the amplitude deterioration in the ETB with the full-size sample of 46% (cf. Figure 10b, gray line) at 1.2 Hz and in the SGB of 45−70% at 1.2 Hz (cf. Figure 8a gray and black lines). It has been demonstrated that reduced back-mixing of the lean-rich switches upstream of the catalysts also results in an increase in the optimal frequency. This is due to the fact that the optimal frequency of the intrinsic kinetic is superimposed with amplitude deterioration.[17,59] Moreover, the 35 K higher temperature difference between the inlet and outlet of the AETB, as illustrated in Figure 12b, at an inlet temperature of 310 °C underscores the high potential of periodic operation for rapid heating of the catalyst to operational temperature.

https://doi.org/10.1021/acs.iecr.5c00132
Ind. Eng. Chem. Res. 2025, 64, 8143−8155

CONCLUSIONS

In this study, a synthetic gas test bench, an engine test bench, and an adaptive engine test bench were employed to assess the periodic operation of an industrially relevant three-way catalyst sample. Herewith, the present study aims at bridging the gap between laboratory-scale and real-world applications, which ensures that theoretical expectations and model-like experimental knowledge can be translated into practical, reliable results in actual engine environments.

The testing of a mini-size catalyst in the SGB provided a controlled environment with precisely set inlet temperatures, gas mixtures, and GHSV, allowing for the evaluation of catalyst activity and rate enhancement from periodic operation. It was observed that periodic operation with an optimal frequency of 1.2 Hz led to a 50% increase in CO conversion and a 90% increase in C_3H_6 conversion at a temperature of 200 °C. Additionally, at a temperature of 250 °C and an optimal frequency of 2 Hz, C_3H_8 conversion increased by 90% and NO conversion by 70% compared to conventional steady-state operation. At the same time, it was possible to enhance N_2 selectivity in a temperature range from 200 to 350 °C by up to 35%.

Despite the elevated exhaust temperature and mass flow, which result from high load conditions and the close coupling of the TWC converter, lower optimal frequencies are observed in the engine test bench that was equipped with the full-size catalyst. The deviations between what was expected based on lab-scale testing and the measurements in the actual engine and tailpipe configurations can be attributed to the inaccurate control of the mean AFR value by the ECU and AFR sensor. Nevertheless, a NO conversion enhancement of 22−29% could be attributed to periodic operation at near stoichiometric conditions. Moreover, the close coupling of the catalyst is highly effective in minimizing amplitude mixing due to axial dispersion in the exhaust tract, thereby enabling a wide frequency range for periodic operation of the TWC.

In order to test the catalyst at low temperatures with minimal back-mixing upstream of the catalyst and under precisely controlled conditions, an AETB was utilized. This setup allows for the measurement of periodic catalyst operation using real exhaust gases at low temperatures, which is particularly important because periodic operation at low temperatures is considered highly effective in the abatement of pollutant emissions during cold starts. The data from the engine test bench corroborate the enhanced pollutant conversion at low temperatures and demonstrate, in line with the data from the two other test benches, that in addition to the direct effect of enhanced pollutant conversion, periodic operation is also advantageous for rapidly reaching operating temperatures that are sufficiently high for ensuring high catalytic activity.

In conclusion, periodic operation offers a promising avenue to enhance exhaust gas catalyst efficiency because it ensures optimal pollutant conversion while adapting to varying engine conditions. The transition from synthetic gas test bench testing to engine test bench testing is a pivotal step in the development of catalyst operation procedures. Consequently, it is of utmost importance to harmonize the operation characteristics of the engine in conjunction with the catalyst formulation and its optimal operating point when developing a periodically operated TWC. By understanding and overcoming the challenges of this transition, we can drive advancements in catalyst technology, ultimately contributing to cleaner and more efficient automotive engines.

ASSOCIATED CONTENT

Supporting Information

The Supporting Information is available free of charge at https://pubs.acs.org/doi/10.1021/acs.iecr.5c00132.

Fuel characterization; NO_2 formation during SGB experiments; calculation of the mean AFR value; fuel properties of the fuel used in the ETB (Table S1) and AETB (Table S2) experiments; cycle-average NO_2 formation at different inlet temperatures and frequencies in the SGB (Figure S1); influence of potential NH_3 formation at low frequencies on the mean AFR value calculation in the ETB (Figure S2) (PDF)

AUTHOR INFORMATION

Corresponding Author

Patrick Lott − *Institute for Chemical Technology and Polymer Chemistry (ITCP), Karlsruhe Institute of Technology (KIT), Karlsruhe 76131, Germany;* orcid.org/0000-0001-8683-2155; Phone: +49 721 608-42782; Email: patrick.lott@kit.edu; Fax: +49 721 608-44805

Authors

Daniel Hodonj − *Institute for Chemical Technology and Polymer Chemistry (ITCP), Karlsruhe Institute of Technology (KIT), Karlsruhe 76131, Germany*

Koki Umemoto − *Faculty of Science and Engineering, Waseda University, Shinjuku-ku, Tokyo 169-8555, Japan*

Masato Terasawa − *Faculty of Science and Engineering, Waseda University, Shinjuku-ku, Tokyo 169-8555, Japan*

Zexin Yu − *Institute of Internal Combustion Engines (IFKM), Karlsruhe Institute of Technology (KIT), Karlsruhe 76131, Germany;* orcid.org/0009-0001-9664-1122

Uwe Wagner − *Institute of Internal Combustion Engines (IFKM), Karlsruhe Institute of Technology (KIT), Karlsruhe 76131, Germany*

Toshihiro Mori − *Toyota Motor Corporation Higashifuji Research Center, Susono, Shinzuoka 410-1193, Japan*

Hiromasa Nishioka − *Toyota Motor Corporation Higashifuji Research Center, Susono, Shinzuoka 410-1193, Japan*

Takao Mishima − *Denso Corporation, Kariya, Aichi 448-8661, Japan*

Olaf Deutschmann − *Institute for Chemical Technology and Polymer Chemistry (ITCP), Karlsruhe Institute of Technology (KIT), Karlsruhe 76131, Germany;* orcid.org/0000-0001-9211-7529

Thomas Koch − *Institute of Internal Combustion Engines (IFKM), Karlsruhe Institute of Technology (KIT), Karlsruhe 76131, Germany*

Jin Kusaka − *Faculty of Science and Engineering, Waseda University, Shinjuku-ku, Tokyo 169-8555, Japan*

Complete contact information is available at: https://pubs.acs.org/10.1021/acs.iecr.5c00132

Notes

The authors declare no competing financial interest.

ACKNOWLEDGMENTS

The authors thank S. Tomin (IFKM, KIT) for support with the adaptive engine test bench and the sample holder, J. Pesek

and S. Lichtenberg (ITCP, KIT) for support with the synthetic gas test bench, and Y. Sugaya (NextGV, Waseda University) and the members of the Japanese Research Association of Automotive Internal Combustion Engines (AICE) and the German Research Association for Combustion Engine e.V. (FVV) for fruitful discussion in the joint project: "TWC Reaction under High-frequency Lambda Switching." This work was funded by AICE Project-ID p210106 and the German Federal Ministry for Economic Affairs and Climate Action (BMWK) Project-ID 314 EN. D.H., Z.Y., U.W., T.K., O.D., and P.L. acknowledge funding by the Deutsche Forschungsgemeinschaft (DFG, German Research Foundation)—SFB 1441—Project-ID 426888090.

■ ABBREVIATIONS

AETB	adaptive engine test bench
AFR	air−fuel equivalence ratio
ECU	engine control unit
ETB	engine test bench
GHSV	gas hourly space velocity
HC	hydrocarbons
HEV	hybrid electric vehicle
ICE	internal combustion engine
OSCC	oxygen storage capacity complete
OSM	oxygen storage material
SGB	synthetic gas test bench
TWC	three-way catalyst
THC	total hydrocarbons

■ REFERENCES

(1) Cho, B. K. Performance of platinum/alumina catalysts in automobile engine exhaust with oscillatory air/fuel ratio. *Ind. Eng. Chem. Res.* **1988**, *27*, 30−36.

(2) Hegedus, L. Poison-resistant catalysts for the simultaneous control of hydrocarbon, carbon monoxide, and nitrogen oxide emissions. *J. Catal.* **1979**, *56*, 321−335.

(3) Herz, R. K.; Kiela, J. B.; Sell, J. A. Dynamic behavior of automotive catalysts. 2. Carbon monoxide conversion under transient air fuel ratio conditions. *Ind. Eng. Chem. Prod. Res. Dev.* **1983**, *22*, 387−396.

(4) Schlatter, J. C.; Sinkevitch, R. M.; Mitchell, P. J. Laboratory reactor system for three-way automotive catalyst evaluation. *Ind. Eng. Chem. Prod. Res. Dev.* **1983**, *22*, 51−56.

(5) Taylor, K. C.; Sinkevitch, R. M. Behavior of automobile exhaust catalysts with cycled feedstreams. *Ind. Eng. Chem. Prod. Res. Dev.* **1983**, *22*, 45−51.

(6) Nakase, T.; Hattori, T.; Naito, J.; Kondo, K. Method of Operating a Three-Way Catalyst for Internal Combustion. U.S. Patent US4199938A1980.

(7) Matsunaga, S.-i.; Yokota, K.; Muraki, H.; Fujitani, Y. *Improvement of Engine Emissions Tower Three-Way Catalyst by the Periodic Operations*; SAE Technical Paper, 1989; p 872098.

(8) Muraki, H.; Shinjoh, H.; Sobukawa, H.; Yokota, K.; Fujitani, Y. Behavior of automotive noble metal catalysts in cycled feedstreams. *Ind. Eng. Chem. Prod. Res. Dev.* **1985**, *24*, 43−49.

(9) Muraki, H. *Performance of Palladium Automotive Catalysts*; SAE Technical Paper, 1991; p 910842.

(10) Yokota, K.; Muraki, H.; Fujitani, Y. *Rh-Free Three-Way Catalysts for Automotive Exhaust Control*; SAE Technical Paper, 1985; p 850129.

(11) Silveston, P. L. Automotive exhaust catalysis under periodic operation. *Catal. Today* **1995**, *25*, 175−195.

(12) Silveston, P. L. Automotive exhaust catalysis: Is periodic operation beneficial? *Chem. Eng. Sci.* **1996**, *51*, 2419−2426.

(13) Zeng, F.; Finke, J.; Olsen, D.; White, A.; Hohn, K. L. Modeling of three-way catalytic converter performance with exhaust mixtures from dithering natural gas-fueled engines. *Chem. Eng. J.* **2018**, *352*, 389−404.

(14) Wang, M.; Dimopoulos Eggenschwiler, P.; Franken, T.; Ferri, D.; Kröcher, O. Reaction pathways of methane abatement in Pd-Rh three-way catalyst in heavy duty applications: A combined approach based on exhaust analysis, model gas reactor and DRIFTS measurements. *Chem. Eng. J.* **2021**, *422*, 129932.

(15) Karinshak, K.; Chen, P. W.; Liu, R.-F.; Golden, S. J.; Harold, M. P. Optimizing feed modulation for coupled methane and NOx conversion over Pd-Pt/$Mn_{0.5}Fe_{2.5}O_4$/Al_2O_3 monolith catalyst. *Appl. Catal., B* **2022**, *304*, 120607.

(16) Deka, D. J.; Pihl, J. A.; Thomas, C. R.; Partridge, W. P. Intra-catalyst CH_4 oxidation pathways on a Pd/Al_2O_3/$CeZrO_x$-based commercial catalyst and implications on NOx conversion profiles for a natural gas vehicle exhaust under lambda modulation. *Chem. Eng. J.* **2023**, *472*, 144803.

(17) Hodonj, D.; Borchers, M.; Zeh, L.; Hoang, G. T.; Tischer, S.; Lott, P.; Deutschmann, O. Impact of operation parameters and lambda input signal during lambda-dithering of three-way catalysts for low-temperature performance enhancement. *Appl. Catal., B* **2024**, *345*, 123657.

(18) Hodonj, D.; Thiele, B.; Deutschmann, O.; Lott, P. Temperature-dependent frequency control of TWC operation for efficient CH_4 and NO_x abatement of stoichiometric natural gas engines. *Chem. Eng. J.* **2024**, *499*, 155852.

(19) Karamitros, D.; Ibraimova, A.; Konstantinidis, K.; Koltsakis, G.; Choi, S.; Cho, J. et al. *Methane Conversion in Stoichiometric Natural Gas Engine Exhaust*; SAE Technical Paper, 2024; p. 2024-01-2632.

(20) Shi, X.; Seiser, R.; Chen, J.-Y.; Dibble, R.; Cattolica, R. Fuel-Dithering Optimization of Efficiency of TWC on Natural Gas IC Engine. *SAE Int. J. Engines* **2015**, *8*, 1246−1252.

(21) Reihani, A.; Fisher, G. B.; Hoard, J. W.; Theis, J. R.; Pakko, J. D.; Lambert, C. K. Rapidly pulsed reductants for diesel NOx reduction with lean NOx traps: Effects of pulsing parameters on performance. *Appl. Catal., B* **2018**, *223*, 177−191.

(22) Schlatter, J. C.; Mitchell, P. J. Three-Way Catalyst Response to Transients. *Ind. Eng. Chem. Prod. Res. Dev.* **1980**, *19*, 288−293.

(23) Mejía-Centeno, I.; Castillo, S.; Fuentes, G. A. Enhanced emissions of NH_3, N_2O and H_2 from a Pd-only TWC and supported Pd model catalysts: Light-off and sulfur level studies. *Appl. Catal., B* **2012**, *119*−*120*, 234−240.

(24) Wang, J.; Chen, H.; Hu, Z.; Yao, M.; Li, Y. A Review on the Pd-Based Three-Way Catalyst. *Catal. Rev.* **2015**, *57*, 79−144.

(25) Huang, C.; Shan, W.; Lian, Z.; Zhang, Y.; He, H. Recent advances in three-way catalysts of natural gas vehicles. *Catal. Sci. Technol.* **2020**, *10*, 6407−6419.

(26) Kaneeda, M.; Iizuka, H.; Hiratsuka, T.; Shinotsuka, N.; Arai, M. Improvement of thermal stability of NO oxidation Pt/Al_2O_3 catalyst by addition of Pd. *Appl. Catal., B* **2009**, *90*, 564−569.

(27) Machida, M.; Fujiwara, A.; Yoshida, H.; et al. Deactivation Mechanism of Pd/CeO_2−ZrO_2 Three-Way Catalysts Analyzed by Chassis-Dynamometer Tests and in Situ Diffuse Reflectance Spectroscopy. *ACS Catal.* **2019**, *9*, 6415−6424.

(28) Yamakawa, Y.; Inoue, R.; Kubo, Y.; Yamaguchi, K.; Kusaka, J. *Conversion Performance Prediction of Thermal-Deteriorated Three-Way Catalysts: Surface Reaction Model Development Considering Platinum Group Metals and Co-Catalyst*; SAE Technical Paper, 2021; p 2021-24-0077.

(29) Tanabe, T.; Nagai, Y.; Hirabayashi, T.; Takagi, N.; Dohmae, K.; Takahashi, N.; Matsumoto, S.; Shinjoh, H.; Kondo, J. N.; Schouten, J. C.; Brongersma, H. H. Low temperature CO pulse adsorption for the determination of Pt particle size in a Pt/cerium-based oxide catalyst. *Appl. Catal., A* **2009**, *370*, 108−113.

(30) Bergeret, G.; Gallezot, P. *Handbook of Heterogeneous Catalysis*; Ertl, G.; Knözinger, H.; Schüth, F.; Weitkamp, J., Eds.; Wiley-VCH Verlag GmbH & Co. KGaA: Weinheim, 2008; Vol. 7, pp 738−765.

(31) Nilsson, J.; Carlsson, P.-A.; Martin, N. M.; Adams, E. C.; Agostini, G.; Grönbeck, H.; Skoglundh, M. Methane oxidation over

https://doi.org/10.1021/acs.iecr.5c00132
Ind. Eng. Chem. Res. 2025, 64, 8143−8155

Pd/Al_2O_3 under rich/lean cycling followed by operando XAFS and modulation excitation spectroscopy. *J. Catal.* **2017**, *356*, 237−245.
(32) Padeste, L.; Baiker, A. Three-Way Catalysts in a Hybrid Drive System: 1. Experimental Study of Dynamic Behavior. *Ind. Eng. Chem. Res.* **1994**, *33*, 1113−1119.
(33) Jiang, X.; Fan, J.; Xiang, S.; Mou, J.; Yao, P.; Jiao, Y.; Wang, J.; Chen, Y. Superior catalytic activity and high thermal durability of $MgAl_2O_4$ modified $Pt/Ce_{0.5}Zr_{0.5}O_2$ TWC. *Appl. Surf. Sci.* **2022**, *578*, 151915.
(34) Wang, C.; Xia, W.; Yang, D.; Zheng, T.; Rong, Y.; Du, J.; Wu, B.; Zhao, Y. Understanding ammonia and nitrous oxide formation in typical three-way catalysis during the catalyst warm-up period. *J. Hazard. Mater.* **2022**, *438*, 129553.
(35) Katare, S. R.; Laing, P. M. Hydrogen in diesel exhaust: effect on diesel oxidation catalyst flow reactor experiments and model predictions. *SAE Int. J. Fuels Lubr.* **2009**, *2*, 605−611.
(36) Rappé, K. G.; DiMaggio, C.; Pihl, J. A.; Theis, J. R.; Oh, S. H.; Fisher, G. B.; Parks, J.; Easterling, V. G.; Yang, M.; Stewart, M. L.; Howden, K. C. Aftertreatment Protocols for Catalyst Characterization and Performance Evaluation: Low-Temperature Oxidation, Storage, Three-Way, and NH_3-SCR Catalyst Test Protocols. *Emiss. Control Sci. Technol.* **2019**, *5*, 183−214.
(37) Tomin, S.; Keller, K.; Wagner, U.; Lott, P.; Koch, T.; Deutschmann, O. Innovative engine test bench set-up for testing of exhaust gas aftertreatment and detailed gas species analysis for CNG-SI-operation. *Automot. Engine Technol.* **2024**, *9*, 2.
(38) Tomin, S.; Wagner, U.; Koch, T. *Effect of Dithering on Post-Catalyst Exhaust Gas Composition and on Short Time Regeneration of Deactivated PdO/Al_2O_3 Catalysts under Real Engine Conditions*; SAE Technical Paper, 2024; p 2024-37-0002.
(39) Takeguchi, T.; Manabe, S.; Kikuchi, R.; Eguchi, K.; Kanazawa, T.; Matsumoto, S.; Ueda, W. Determination of dispersion of precious metals on CeO_2-containing supports. *Appl. Catal., A* **2005**, *293*, 91−96.
(40) Phan, D. Q.; Kureti, S. CO oxidation on Pd/Al_2O_3 catalysts under stoichiometric conditions. *Top. Catal.* **2017**, *60*, 260−265.
(41) Shen, M.; Yang, M.; Wang, J.; Wen, J.; Zhao, M.; Wang, W. Pd/Support Interface-Promoted $Pd−Ce_{0.7}Zr_{0.3}O_2−Al_2O_3$ Automobile Three-Way Catalysts: Studying the Dynamic Oxygen Storage Capacity and CO, C_3H_8, and NO Conversion. *J. Phys. Chem. C* **2009**, *113*, 3212−3221.
(42) Li, P.; Chen, X.; Li, Y.; Schwank, J. W. A review on oxygen storage capacity of CeO_2-based materials: Influence factors, measurement techniques, and applications in reactions related to catalytic automotive emissions control. *Catal. Today* **2019**, *327*, 90−115.
(43) Keitl, G.; Rink, J.; Wen, F.; Jongen, L.; Hofmann, A.; Votsmeier, M.; Terfort, A.; Gieshoff, J. Impact of Test Conditions on the Oxygen Storage Capacity of Pd Loaded Cerium Zirconium Oxide. *Top. Catal.* **2017**, *60*, 272−277.
(44) Rink, J.; Meister, N.; Herbst, F.; Votsmeier, M. Oxygen storage in three-way-catalysts is an equilibrium controlled process: Experimental investigation of the redox thermodynamics. *Appl. Catal., B* **2017**, *206*, 104−114.
(45) Dhainaut, F.; Pietrzyk, S.; Granger, P. NO + H_2 reaction on Pd/Al_2O_3 under lean conditions: kinetic study. *Top. Catal.* **2007**, *42*−*43*, 135−141.
(46) Malamis, S. A.; Li, M.; Epling, W. S.; Harold, M. P. Steady state and lean-rich cycling study of a three-way NO_X storage catalyst: Experiments. *Appl. Catal., B* **2018**, *237*, 588−602.
(47) Getsoian, A. B.; Theis, J. R.; Lambert, C. K. Sensitivity of Three-Way Catalyst Light-Off Temperature to Air-Fuel Ratio. *Emiss. Control Sci. Technol.* **2018**, *4*, 136−142.
(48) Qian, Y.; Wei, X.; Sun, Y.; Tang, F.; Meng, S.; Qiu, L.; Wang, T.; Ye, B.; Pan, T.; Zhang, Y. Investigation of the formation characteristics of N_2O and NH_3 for stoichiometric natural gas engines with Pd-only catalyst. *Fuel* **2022**, *329*, 125223.
(49) Cutlip, M. B. Concentration forcing of catalytic surface rate processes: Part I. Isothermal carbon monoxide oxidation over supported platinum. *AIChE J.* **1979**, *25*, 502−508.
(50) Carlsson, P.-A.; Mollner, S.; Arnby, K.; Skoglundh, M. Effect of periodic operation on the low-temperature activity for propane oxidation over Pt/Al_2O_3 catalysts. *Chem. Eng. Sci.* **2004**, *59*, 4313−4323.
(51) Barshad, Y.; Gulari, E. A novel catalytic reactor system for transient response and its use in CO oxidation on Pd/Al_2O_3. *J. Catal.* **1985**, *94*, 468−477.
(52) Zhou, X.; Barshad, Y.; Gulari, E. Co oxidation on Pd/Al_2O_3. Transient response and rate enhancement through forced concentration cycling. *Chem. Eng. Sci.* **1986**, *41*, 1277−1284.
(53) Rajagopalan, S. S.; Midlam-Mohler, S.; Yurkovich, S.; Dudek, K. P.; Guezennec, Y. G.; Meyer, J. A control design and calibration reduction methodology for AFR control in gasoline engines. *Control Eng. Pract.* **2014**, *27*, 42−53.
(54) Buglass, J. G.; Morgan, T.; Graupner, J. Interactions between exhaust gas composition and oxygen sensor performance. *SAE Trans.* **1998**, *107*, 1930−1940.
(55) Cho, B. K.; West, L. A. Cyclic operation of platinum/alumina catalysts for carbon monoxide oxidation. *Ind. Eng. Chem. Fundam.* **1986**, *25*, 158−164.
(56) Hu, Z.; Wan, C.; Lui, Y.; Dettling, J.; Steger, J. Design of a novel Pd three-way catalyst: integration of catalytic functions in three dimensions. *Catal. Today* **1996**, *30*, 83−89.
(57) Werther, M.; Singer, C.; Gross, A.; Kureti, S.; Martínez-Munuera, J. C.; García-García, A. Effect of SO_2 on the soot oxidation activity of flame spray pyrolysis-made manganese oxide catalyst in gasoline model exhaust. *React. Kinet., Mech. Catal.* **2024**, *137*, 1455−1469.
(58) Wang, M.; Li, S.; Zhu, R.; Zhang, R.; Zu, L.; Wang, Y.; Bao, X. On-road tailpipe emission characteristics and ozone formation potentials of VOCs from gasoline, diesel and liquefied petroleum gas fueled vehicles. *Atmos. Environ.* **2020**, *223*, 117294.
(59) Reihani, A.; Patterson, B.; Hoard, J. W.; Fisher, G. B. Global kinetic modeling of rapidly pulsed reductants for lean NOx traps: Frequency domain analysis and impact of mass transfer. *Appl. Catal., B* **2019**, *254*, 223−236.

https://doi.org/10.1021/acs.iecr.5c00132
Ind. Eng. Chem. Res. 2025, 64, 8143−8155